PAPER • OPEN ACCESS

An assessment of contamination pickup on ground robotic vehicles for nuclear surveying application

To cite this article: A Banos *et al* 2021 *J. Radiol. Prot.* **41** 179

View the article online for updates and enhancements.

An assessment of contamination pickup on ground robotic vehicles for nuclear surveying application

A Banos[1] , J Hayman[1], T Wallace-Smith[1], B Bird[2], B Lennox[2] and T B Scott[1]

[1] University of Bristol, Interface Analysis Centre, School of Physics, HH Wills Physics Laboratory, Tyndall Avenue, Bristol BS8 1TL, United Kingdom
[2] University of Manchester, School of Electrical and Electronic Engineering, Manchester M13 9PL, United Kingdom

E-mail: antonis.banos@bristol.ac.uk and antonisbanos@gmail.com

CrossMark

Abstract

Ground robotic vehicles are often deployed to inspect areas where radioactive floor contamination is a prominent risk. However, the accuracy of detection could be adversely affected by enhanced radiation signal through self-contamination of the robot occurring over the course of the inspection. In this work, it was hypothesised that a six-legged robot could offer advantages over the more conventional ground robotic devices such as wheeled and tracked rovers. To investigate this, experimental contamination testing and computational Monte Carlo simulation techniques (GEANT4) were employed to understand how radioactive contamination pick-up on three different robotic vehicles would affect their detection accuracy. Two robotic vehicles were selected for comparison with the hexapod robot based on their type of locomotion; a wheeled rover and a tracked rover. With the aid of a non-toxic fluorescent tracer dust, the contamination received by the all three vehicles when traversing a contaminated area was initially compared through physical inspection using high definition cameras. The parametric results from these tests where used in the computational study carried out in GEANT4. A cadmium zinc telluride detector was simulated at heights ranging from 10 to 50 cm above each contaminated vehicle, as if it were mounted on a plinth. Assuming a uniform activity of 60 Bq cm^{-2} on all contaminated surfaces, the results suggested

that due to the hexapod's small ground-contacting surface area and geometry, radiation detection rates using an uncollimated detector are likely to be over-estimated by between only 0.07%–0.12%, compared with 3.95%–8.43% and 1.75%–14.53% for the wheeled and tracked robot alternatives, respectively.

Keywords: hexapod robot, ground inspection, robot self-contamination, radiation mapping

(Some figures may appear in colour only in the online journal)

1. Introduction

In many industries where toxic materials and wastes are produced, unmanned robotic vehicles are commonly used to inspect hazardous areas of plants which would otherwise be risky or impractical for humans to investigate [1, 2]. In the nuclear industry, high resolution inform-ation regarding the locations and intensities of radioactivity is vital for developing safe and cost-effective strategies for clean-up and decommissioning of plants and building structures. Assessment and quantification of facilities which contain loose radioactive particulates, often small enough to be aerosolised, is both challenging and risky for human workers since the dust material that is suspended within the contaminated area, and contain radionuclides, can be physically disturbed by worker activities and result in their contamination [3].

In order to obtain reliable data with regards to radioactive contamination within these areas, the 'hotspots' or high radiation intensity locations must be initially identified through timely inspections. At a later stage and in order to obtain high resolution maps, collimated and direc-tional radiation detection, which requires long exposure times, can be employed on the areas of interest. For both actions, a purpose-built unmanned robotic vehicle loaded with the appro-priate instrumentation becomes a valuable tool since it reduces to minimum the health and safety risk of having humans undertaking this task [4]. The extensive use of robotics for nuc-lear applications has been demonstrated since the 2011 Fukushima Daichii nuclear accident where the emerging challenge of inspection and determination of radioactivity was met with the deployment of a wide variety of unmanned robotic vehicles [5–10]. Of course, working in the immediate vicinity of a melted reactor core is about as extreme as it gets. More 'routine' operations would include the decommissioning of nuclear power plants, fuel reprocessing facilities, waste repositories and related legacy buildings [11]. In these facilities, contrary to nuclear accident sites, the highly 'active' material is expected to be found in site-specific loc-ations, with large areas likely to be only lightly contaminated, if contaminated at all. This generates the need to produce sensitive detection and characterisation systems capable of find-ing and reporting areas of elevated radiation intensity (versus background) whilst distinguish-ing between naturally occurring radiation versus gamma-radiation originating from human activities.

For environments where ground contact is not desirable, an unmanned aerial vehicle could serve as an ideal solution [12–15]. However, for enclosed indoor environments with 'active' particulate contamination, the substantial downdraught of a typical propeller-powered drone combined with the size and load-carrying capacity ratio make them unsuitable for this work. Furthermore, low-activity radiation detection becomes much more difficult when flying due to battery constraints and corrections required for altitude, making aerial mapping more suited to outdoor use [15]. Tracked rovers [5, 16, 17], wheeled rovers [18, 19], pipe-crawlers [20–22], vertical crawlers [23, 24] and other robotic types [25] could be used as ground robotic devices for surveying and gamma radiation inspection. With respect to ground robots, the

amount of contamination any robotic vehicle shall receive from ground-based particulate matter is highly likely to be linked to the surface area of the robot that comes into contact with the floor, as well as the type of motion. A system which would not spread contamination to previously uncontaminated areas or become excessively contaminated itself, leading to inaccurate radiation readings, would be preferable. In this respect, walking robots, which have minimal area contact with the ground, offer an attractive solution for limiting contamination pick-up during surveys and manual operations [26, 27]. It was hypothesised that, compared to traditional tracked and wheeled vehicles, a hexapod robotic system would become less contaminated during deployment in facilities with floor-based contamination in the form of micro-scale radioactive particulates or 'active' dust. By minimising the spread of hazardous material and contamination pick-up on the device, the quality of the overall characterisation of the surveyed environment would significantly improve. In this work, we will therefore investigate how contamination pick-up is likely to occur on the various robotic devices and understand how it will affect the radiation mapping data of an on-board radiation detector. There is no prior literature on conducting such an analysis, and hence this work is both novel but potentially important for informing the selection of robot platform used for different nuclear inspections.

2. Experimental methods

Three robotic systems have been tested in this work, each with a distinctly different method of locomotion. It is important to note that for the contamination pick-up experiments the robots were tested largely unmodified. It is suggested that integration of equipment, such as sensors, detectors, and cameras, would not affect our study.

2.1. Wheeled rover

The wheeled robot used in this work is a four-wheeled remote-control robot, known as a 'Leo Rover' which was designed by Kell ideas Ltd (figure 1) [28]. It incorporates a rocker design to improve traction over rough terrain, similar to NASA's Mars rovers [29]. Each wheel is driven by an independent in-hub motor and similarly to the tracked rover, the wheels are fixed, and steering is achieved by torque differential between the motors.
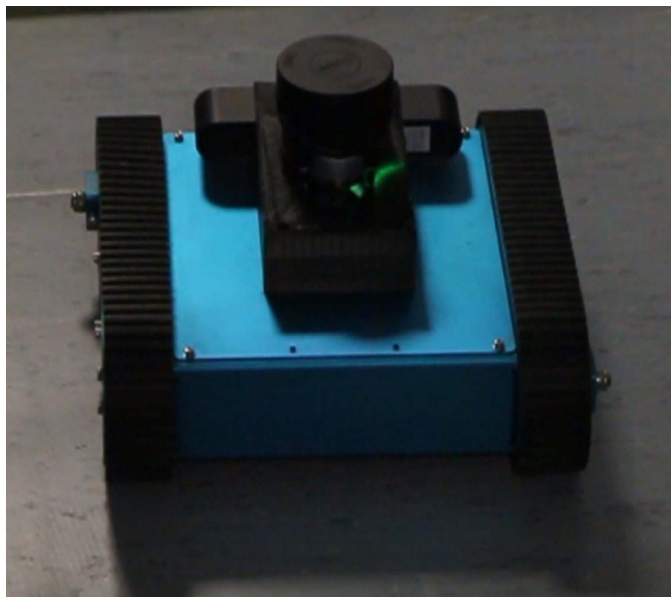
2.2. Tracked rover

Figure 2 displays the tracked rover used for testing which is based on the twin-track differential steering platform from Nexus automation Ltd [30]. The unit is custom-modified and includes a light detection and ranging mapping system and a retractable power and control wiring spool. Motors and circuitry are housed within a protective aluminium casing.

2.3. Hexapod robot

The hexapod is a six-legged robot with an aluminium frame platform and is based on the Phantom AX metal Hexapod MK-III designed from Interbotix labs (figure 3) [31]. This is an off-the-shelf kit that comes as a collaborative effort from Next-Gen AX Dynamixel robot servos and the Arbotix-M robocontroller. Locomotion is achieved with 18 Dynamixel AX-18A electric robot actuators, connected to an onboard computer which is loaded with open source software (Phoenix code). Remote control can be wireless or wired and power can be supplied either by lithium-polymer batteries or through hardwiring. Rubber ferrules are fitted in the bottom side of each leg of the robot to enhance motion stability and protect the robot
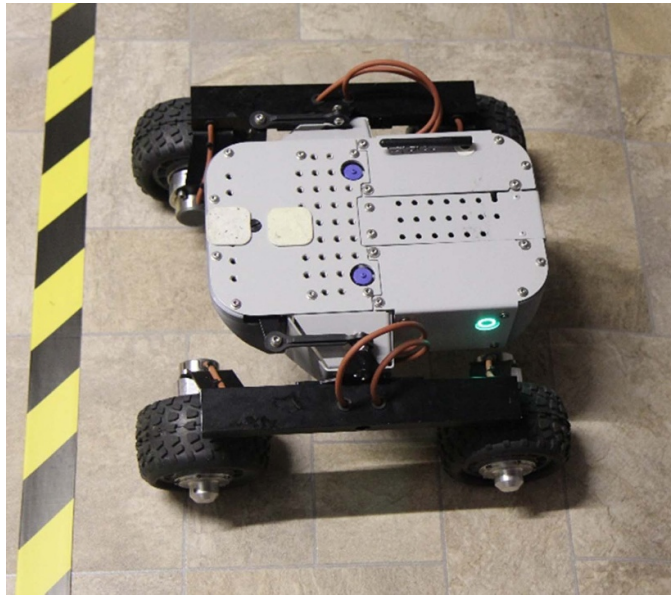
Figure 1. Photographic image showing the four-wheel 'Leo Rover' from Kell ideas limited.

Figure 2. Photographic image showing the tracked rover from Nexus automation limited.

from ground contamination. Table 1 presents the operational parameters of the three robot platforms.

Table 1. Operational parameters of the three robots.

Robot platform	Powel supply	Control mechanism	Mass	Locomotion mechanism	Load carrying capacity
Wheeled rover	11.1 V DC, 2 A max current per wheel (4× servos)	Wireless control	6.5 kg	Rolling (Four wheels)	5 kg
Tracked rover	11.1 V DC, 1.5 A max current per servo (2× servos)	Wireless commander	5 kg	Tracked robot	5.5 kg
Hexapod robot	11 V DC, 2.2 A max current per servo (18× servos)	Wireless Xbee control via PC or handheld	⩾2 kg	Walking (Six-legged robot)	2.1 kg

Figure 3. Photographic image of the off-the-shelf Phantom AX metal Hexapod MK-III by Interbotix lads. In this image a LIDAR and radiation detector are integrated to the robot.

2.4. Contamination tests—experimental procedure

The main objective of the experimental analysis was to create a simulated environment with floor-based contamination and examine/compare the contamination pick-up of the robots after exiting this designated area. To simulate contamination in the form of fine radioactive dust, the designated floor area was uniformly covered with a layer of fluorescent micro-scale powder. For the simulation, a Romax fluorescent tracking powder from Pestfix pest control supplies was used [32].

A flat (1.2 × 1.2 m) surface was selected for the experimental tests. The surface was sufficiently large to allow the robots to complete at least one full 360° rotation whilst traversing and before exiting to the clean side. The experimental area was sprinkled with fluorescent powder uniformly at a density of ~50 g m^{-2} using a sieve.

Before each experimental run each robot was thoroughly cleaned and inspected under UV light with photos being taken under visible and UV light from various angles. The robot was then placed immediately adjacent to the designated contamination area in order to start the contamination test. Individually, each robot was then piloted in a straight line through the designated and into the bounding 'clean' zone on the far side. The robot was then turned-off, carefully collected from the exit area, and placed on clean laboratory benchtop for inspection. Inspection photos and videos of the robot were recorded, consistent with prior inspections of each clean robot to provide a basis for comparison between their clean and contaminated states. The experimental process was then repeated a second time (after the robot was thoroughly cleaned), but with the robot completing a 360° rotation in the centre of the contaminated space before exiting the designated area.

After exiting the contaminated area, each robot was inspected separately under normal and UV light. High definition photographic images were taken under both illumination sources. The imaging data gathered under UV lighting was the primary data source for contamination analysis. The contaminated surface area from each robot was calculated and related to the overall surface area of the device. These surface area measurements were then used to inform subsequent radiation simulations to assess the effect that different amounts of contamination pick-up would have on an on-board radiation detector carried by each robot.

For the validity of the experiment it was assumed that the test area was sufficiently large and any small variations in the density of fluorescent dust floor coverage would have a negligible effect on the amount of contamination detected on the robots. Negligible effect on the thickness and coverage of the fluorescent dust was also assumed after each experimental run. Airborne contamination of robots through active movement of the dust was negligible and did not contribute to the detectable contamination.

2.5. Radiation modelling

If a robot is carrying a radiation detector for mapping purposes, an accumulation of radioactive contamination onto the platform will provide a variable offset to the radiation measurements at a close proximity, thereby decreasing the accuracy and reliability of the survey data. To computationally model by how much 'hot' contamination pick-up onto the different robot platforms could offset detector measurements, GEANT4 was simulations were utilised. Developed at CERN to efficiently and precisely model particle interactions within the Large Hadron Collider experiment, GEANT4 is a freely available tool for simulating the interactions of particles within matter, coupled with a vast library of experimental physics data describing electromagnetic, nuclear and kinetic processes [33]. GEANT4 allows a user to input geometry, materials and specify particle tracking and interaction detection parameters to produce simulation data. By treating volumes as homogenous materials with definable compositions and densities, particles of specific energy are tracked where reaction cross sections and probability function sampling is utilised to determine reaction rates. In simpler terms, a simulation architecture is set where different objects, detectors and their material and elemental compositions are defined. This architecture is then populated with sources where high energy particles are generated and emitted with their interactions with matter being tracked and counted based on reaction rates derived from experimental data libraries. Data presented in this work were

generated using version 10.4 of GEANT4 with all additional data files using a repurposed version of the 'radioprotection' example model provided with the code.

A model was generated which consisted of a 1.2 m cube full of air with a 10 mm cube Cadmium zinc telluride (CZT) detector at its centre to represent a typical micro-gamma spectrometer detector used on a survey robot. The detector, designed from Kromek, has an operating energy range of 30 keV to 3 MeV with maximum throughput of 30 000 counts per second. Radioactive contamination was modelled for each robot type as a series of distributed surface sources approximating the track, wheel or footpad dimensions of the different robots. Detector hits were measured as any particle which deposited energy into the CZT bulk, as would be measured by current pulses in the actual detector circuit.

3. Results

3.1. Contamination tests

3.1.1. Wheeled rover.   Figures 4(a)–(f) show images from the wheeled robot contamination tests. From traversing the test area, the rover picked up significant contamination on the four wheels (figures 4(a)–(c)), with an amount of contamination deposited from the robot wheels onto the floor of the adjacent clean area on the exit side (figure 4(b)). Negligible contamination was observed on the main body of the robot at this stage. After the robot was cleaned, a second trial was carried out with the rover completing a full rotation in the centre of the test area (figures 4(d) and (e)). A visibly larger disruption of the contaminated floor area was observed (figure 4(d)) with a commensurately increased amount of contamination was observed on the robot wheels and spread (from the wheels) into the adjacent clean area. Contamination was, again, observed almost exclusively in the four wheels of the robot, though comparison of images between the test runs (figures 4(c) and (e)), indicates that contamination on the wheels was higher in the second trial (full rotation).

3.1.2. Tracked rover.   Figures 5(a)–(f) show images from the tracked vehicle tests. After a simple straight-line traverse of the test area, significant contamination coverage was observed on the two tracks of the robot (figures 5(a) and (b)) with smaller amounts of contamination spread onto the main body of the robot from the movement of the tracks. Larger accumulations of the fluorescent particulate had also become trapped between the track and the tread of the robot. Following the full rotation test, a clear area of contaminant disruption in centre of the 'hot' area was observed with an accompanying trail of ground contamination out into the (initially) clean exit area (figure 5(c)). Such contamination trails were observed for both tests (traversing and full rotation). Robot track contamination and contamination spread onto the body of the robot was more pronounced after a full rotation when compared to a simple straight-line traverse across the test area (figures 5(b) and (d)).

3.1.3. Hexapod robot.   Figures 6(a)–(e) show results from the contamination tests using the hexapod robotic system. After traversing the test area, the robot exhibited localised particulate contamination on the rubber 'foot' ferrules fitted on the basal tip of the legs (figures 6(a)–(c)). Small amounts of spot contamination could be observed on the lowermost 10 mm of the hexapod legs. From the two tests, both resulted in a contamination trail on the exit side of the 'hot' zone, exhibiting a rapidly diminished abundance with increased distance (figure 6(a)). After completing a full rotation within the contaminated area (trial two), some lighter contamination in the lower tibia/leg section was observed, extending to ~50 mm from the tip of each
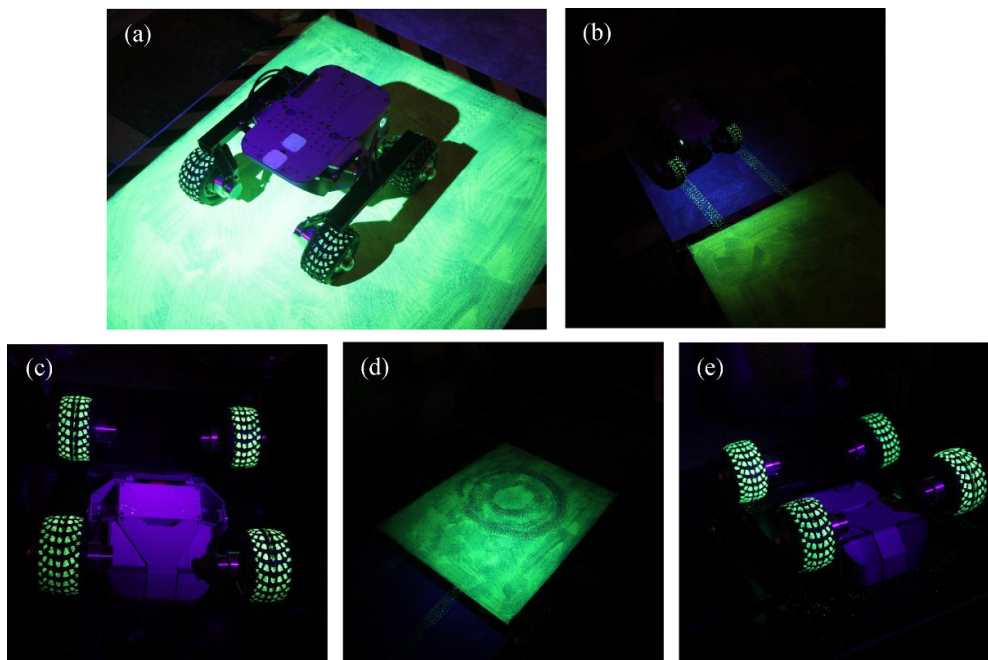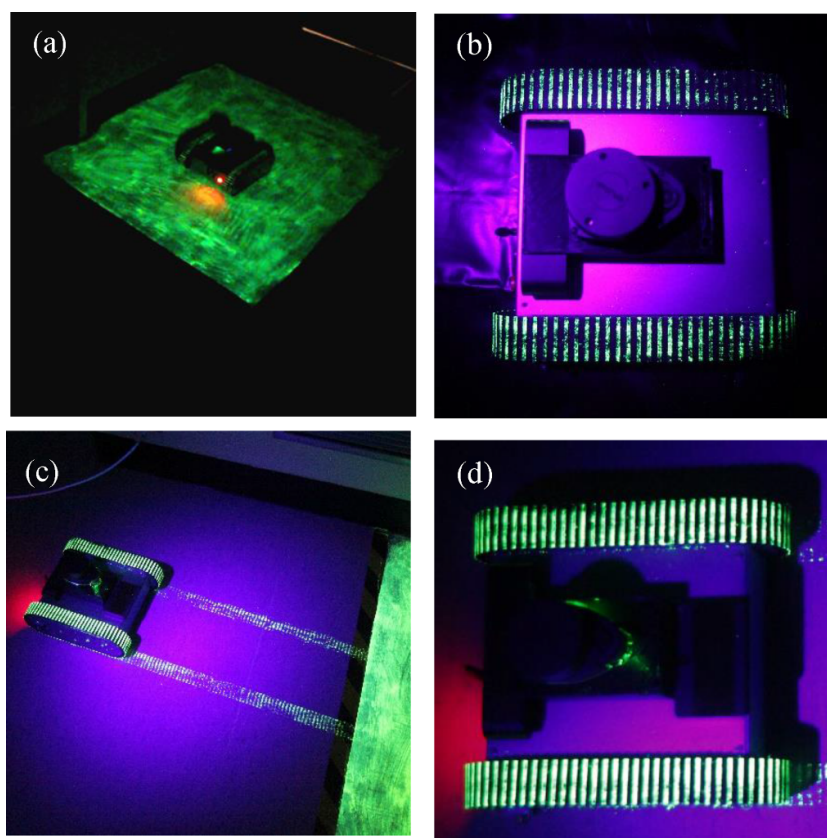
Figure 4. Images showing on (a) the wheeled rover traversing the test area; (b) the markings left on the exit side of the designated environment after trial one (traversing); (c) the contamination picked up on the body of the robot after completing trial one (traversing); (d) the tracking marks of the robot within the test environment after trial two (full rotation) and (e) the contamination picked up on the body of the robot after trial two (full rotation).

leg (figure 6(d)). Sparse, isolated particulates were also observed on parts of the underside of the vehicle. Minimal disruption of the contaminated floor area was observed (figure 6(c)), although the elongated shape of the footprints recorded in the contamination trails indicated that some slippage of around 0.5–1.0 cm has occurred as the robot moved. Figures 6(b) and (e) show that contamination pick-up on the legs and ensuing contamination of the adjacent clean area were increased in the second trial where a full rotation of the robot was executed.

3.2. Contaminated surface area measurement vs radioactivity

The dimensions and the approximated surface areas were calculated for the floor-contacting components of each robot. This was then cross-referenced with the observed coverage of fluorescent dust for each robot. To determine the simulated accumulated radioactivity of each robot, based on their observed contaminated area, it was assumed that the traction surfaces were perfectly flat, i.e. ignoring tread, patterns, etc. This could lead to either underestimation or overestimation of contamination, given that the tread grooves could be covered with dust or be completely clean. However, given the significant difference in surface area between the robotic platforms, the comparisons would still be valid. It was also assumed that contaminated traction-surfaces of the robots had a uniform coating of material. In reality, the amount of contamination would be directly proportional to the thickness and composition of the dust, the pressure exerted by the vehicle and the environmental conditions such as humidity, temperature, etc. Still,
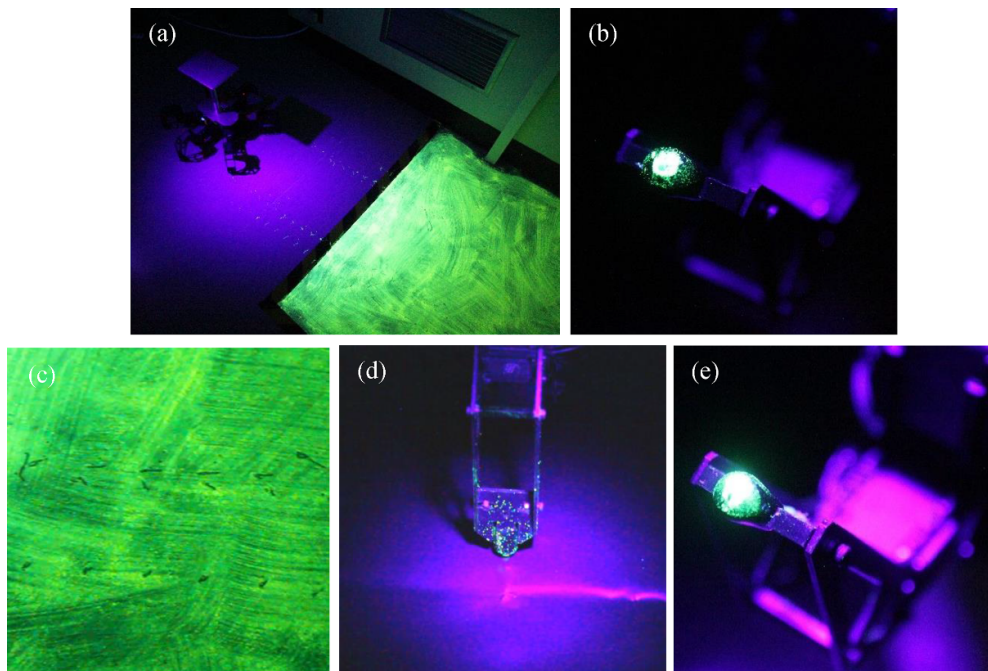
Figure 5. Images showing on (a) the tracked rover traversing the test area; (b) the contamination picked up on the body of the tracked robot after trial one (traversing); (c) the markings left on the exit side of the designated environment after trial two (full rotation) and (d) the contamination picked up on the body of the robot after trial two (full rotation).

the single layer contamination approach was considered a reasonable approximation for the purposes of this work. Table 2 presents the results from this process. The hexapod and wheeled rover yielded a comparable total surface area which was twice that of the tracked rover. However, the contaminated surface area for the hexapod robot was considerably lower in comparison to the other systems (table 2). By assigning an arbitrary radioactivity of 60 kBq cm^{-2} arising from floor contamination, the overall faux radioactivity which was picked up by each robot could be calculated. The results clearly indicated that, with the same level of radioactivity per unit area of contamination, the hexapod exhibits an overall activity which is 56 and 63 times lower than the wheeled and tracked rovers, respectively.

3.3. GEANT4 modelling

A visualisation of the source distribution chosen to represent the contamination of the floor area as well as that of each robot is shown in figures 7–10. In each visualisation, the red particle traces represent energetic electrons produced by the gamma radiation ionising the air within the room. The models of figures 7–10 were run with 10 million gamma particles and 12 repeat runs

Figure 6. Images showing on (a) the markings left on the exit side of the designated environment after trial one (traversing); (b) the contamination picked up on the rubber ferrule at the tip of the leg after trial one (traversing); (c) the tracking marks of the hexapod robot within the designated area after trial one (traversing); (d) the contamination around the tibia section of the robot leg after trial two (full rotation) and (e) the contamination picked up on the rubber ferrule at the tip of the leg after trial two (full rotation).

for each data point with different random seed and by adjusting the distance between the source and detector by 5 cm increments. The results of these simulations were presented in figure 11. The value for detector hits per second was adjusted for the total amount of contamination you would expect on each robot type shown in table 2. The results show the detector hits per second you would expect for homogenous 60 kBq cm^{-2} contamination on the robots and floor.

From figure 11 it can be observed that the majority of detector hits would come from the surrounding floor, the contamination level of which is homogenous. The tracked rover produced a higher signal than that of the wheeled rover but dropped off more quickly with increased detector distance. This was due to the dimensions of the tracked rover having a higher distribution of activity at the top and bottom of the tracks, whereas the wheeled rover approximated more closely to four point-sources. The hexapod exhibited by far the lowest detector hits by comparison, meaning that during a gamma detection measurement in a contaminated plant area the influence on the detector signal due to the robot's self-contamination would be minimal.

For all the simulated sources of gamma radiation; floor, hexapod, tracked and wheeled, the relationship between the number of gamma hits on the CZT detector crystal and its distance above the ground surface (representing different mounting heights above the robot chassis) could be described by an exponential in the form of equation (1):

$$y = A\exp(-Bx),\tag{1}$$

Table 2. Integrating some of the calculated parameters for each robot after the contamination pick-up tests.

	Hexapod	Wheeled rover	Tracked rover
Length (cm)	41	41	31
Width (cm)	44	46	30
Overall surface area (cm^2)	1804	1886	930
Contaminated surface area (cm^2)	9.4	530.9	596.5
Total activity (kBq)	0.56	31.85	35.79
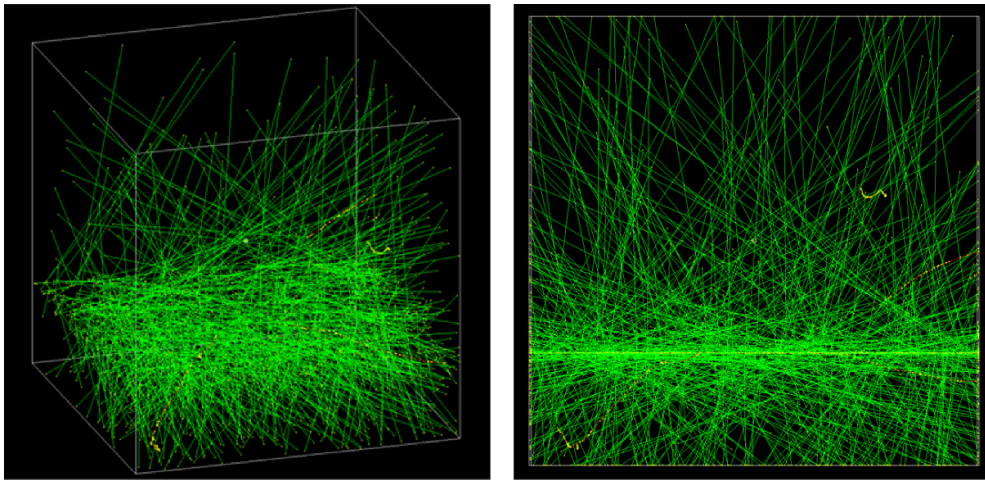
Figure 7. Floor contamination source distribution with the distance between the source and cadmium zinc telluride (CZT) detector set at 30 cm distance. The simulation was run with 10 million gamma particles.

with 'y' in hits per second for 60 kBq cm^{-2} contamination over each surface type. 'A' is the value for hits at $x = 0$ or where there was no distance between the detector and the source (as $\exp(0) = 1$), 'B' was the gradient with which the number of detector hits per second decays with increased simulated detector height, as seen in figure 11. In order to calculate the error caused by each robot type, E, the following equation was used:

$$E = (i/F) \times 100\%, \tag{2}$$

where i is the added erroneous gamma hits influencing the detection measurement of F. The error, E, was therefore calculated as a percentage of the measurement of F. To find a general error equation for a decaying exponent, both i and F could be substituted with their respective decay equations derived from figure 11. Where A_i was the tracked, wheeled and hexapod equations whilst F was the line fitted to the floor contamination measurements. Dividing the two exponentials gives equation (3) as:

$$E_i = (A_i/F)\exp\left(-|B_i - B_F|x\right)100\%. \tag{3}$$
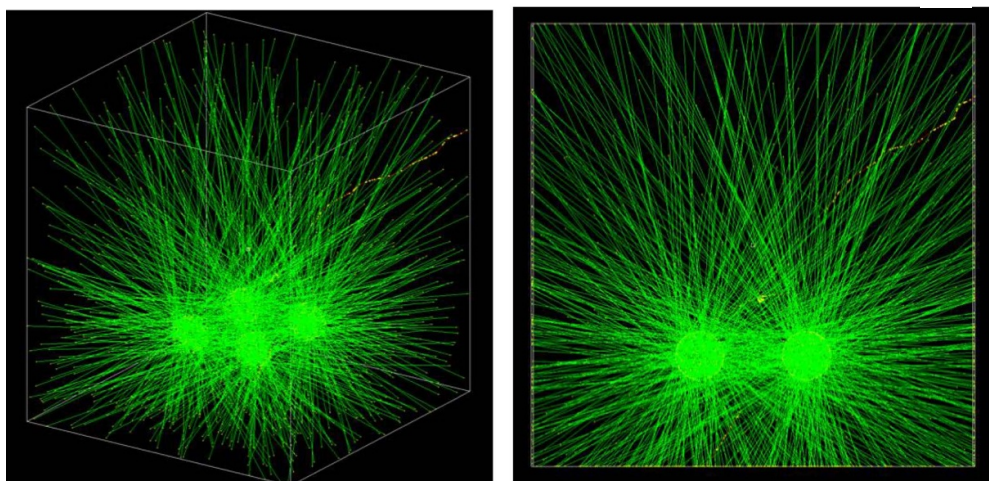
Figure 8. Wheeled robot source distribution with the distance between the source and cadmium zinc telluride (CZT) detector set at 30 cm distance. The simulation was run with 10 million gamma particles.
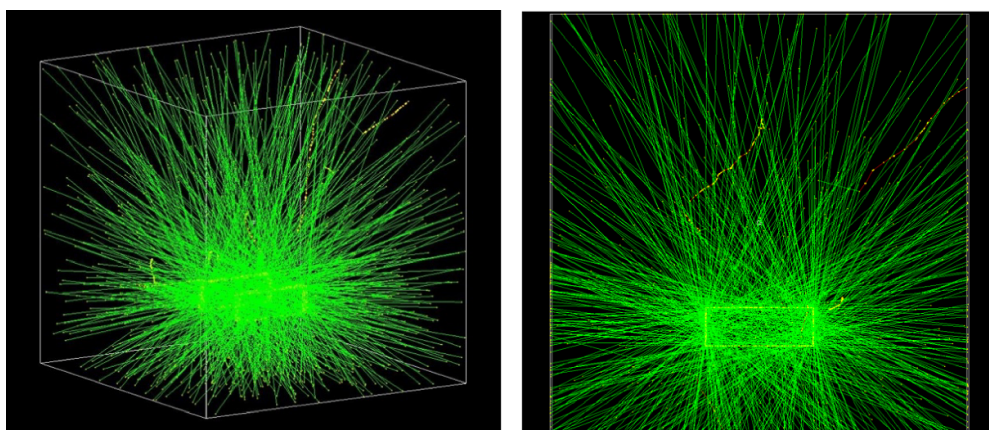
Figure 9. Tracked rover source distribution with the distance between the source and cadmium zinc telluride (CZT) detector set at 30 cm distance. The simulation was run with 10 million gamma particles.

Therefore, the associated error induced by self-contamination on each robot type can be expressed by the following equations:

$$E^{\%}_{\text{Wheel}} = 10.2\mathrm{e}^{-0.019x}, \tag{4}$$

$$E^{\%}_{\text{Tracked}} = 24.7\mathrm{e}^{-0.053x}, \tag{5}$$

$$E^{\%}_{\text{Hexapod}} = 0.14\mathrm{e}^{-0.014x}, \tag{6}$$

where $E^{\%}$ is the percentage error in the detection measurement due to the accumulated contamination on the robot and x is the elevation of the detector above the floor, mounted at different heights on top of the robot. These equations were derived from the fitted exponentials

Figure 10. Hexapod robot source distribution with the distance between the source and cadmium zinc telluride (CZT) detector set at 30 cm distance. The simulation was run with 10 million gamma particles.
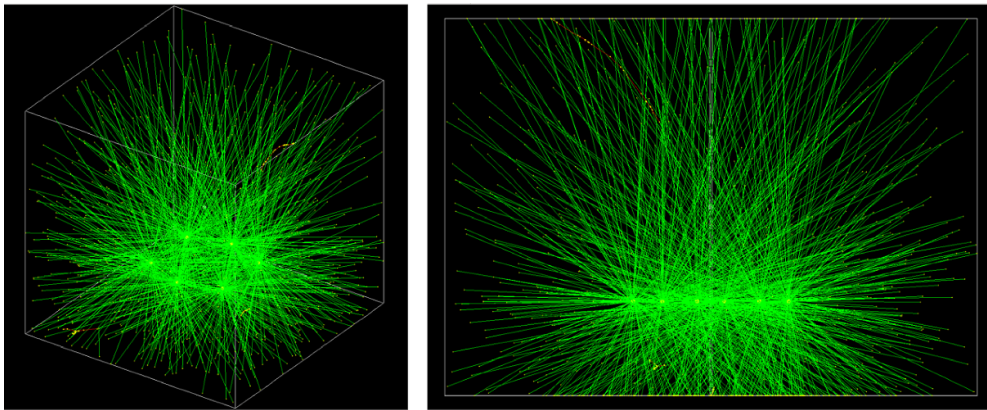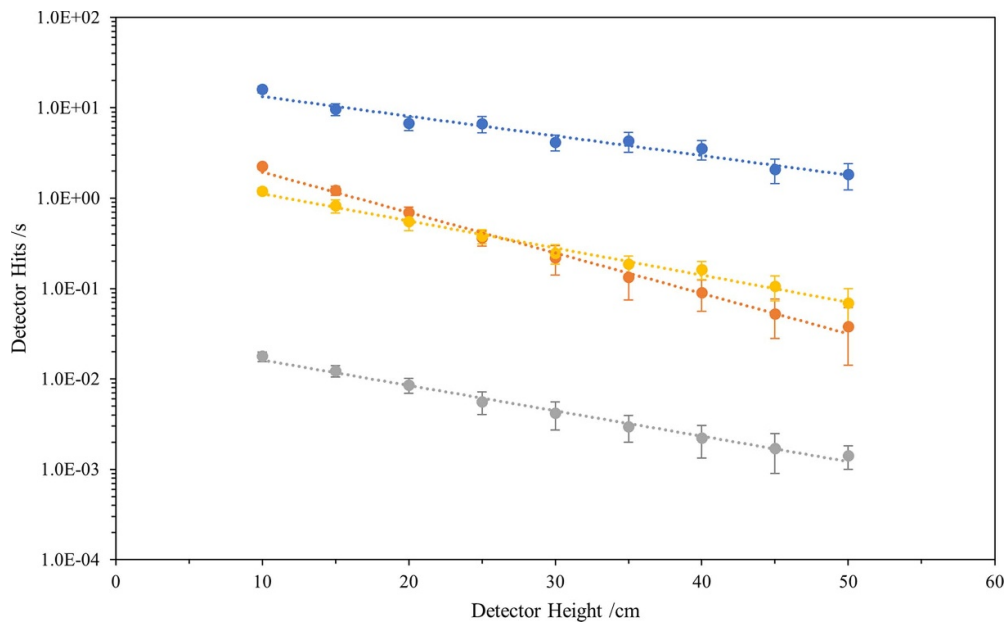

Figure 11. Detector height vs detector hits per second for various active areas of contamination at 60 kBq cm^{-2} Co^{60}; floor (blue), wheeled rover (yellow), caterpillar track rover (orange) and hexapod (grey).

for each robot type shown in figure 11. This showed that at $x = 10$ cm, the signal from the tracked and wheel robots was 119 and 69 times larger, respectively, than that of the hexapod. The first coefficient in equations (4)–(6) are characteristic of the dimensions of the robots and their contaminated surfaces, so the small traction-surface area presented by the hexapod's feet significantly reduced this coefficient and hence reduced the associated erroneous gamma counts that would register on the detector from the accumulated self-contamination.

The second coefficient in the equation's exponent relates to how the intensity of the measured gamma flux on the detector dropped away as it became increasingly elevated above the ground surface; a typical geometrical dilution. These equations could be used to appraise the expected 'contamination performance' of different robot platforms planned for radiation mapping deployments and also to calculate an offset correction to radiation survey measurements where radioactive contamination of a robot is considered to have occurred.

4. Discussion

Robotic vehicle contamination from floor-based radioactive particulates was investigated in this work. To our knowledge, this is the first time that such a study has been conducted to compare contamination pick-up between different robotic systems. By using fluorescent powder as a surrogate to radioactive dust, contamination pick-pup performance could be effectively documented, yielding semi-quantitative results. By comparing the performance of the three robots in trial one (straight-line traversing) it was found that the wheeled and tracked robot contaminated their traction surfaces almost completely after the first revolution of the wheels or tracks. Only minimal further increase in robot contamination was observed as the robots advanced. Similar to the rovers, the hexapod was expected to be fully contaminated in the leg area within the first few steps. In all cases the robots were quick to accumulate contamination.

Performing a full rotation (trial two) resulted in increased disruption of the contaminated floor area and increased particulate pick-up onto the tread of both the tracked and wheeled platforms. There was also a commensurate increase in the amount of contamination trailed out of the test area. By comparison, the hexapod exhibited no significant differences in floor disturbance and contamination trailing between the two experiments. This was ascribed to the rotational manoeuvre causing ostensibly only the same disturbance as if it were walking in a straight line. Only a small increase in contamination was observed around the tibia section of the legs, which was considered negligible when compared to the other robots.

Upon close inspection, all robots in all experiments had a small amount of particulate speckling to areas other than just the traction surfaces, typically on the underside surfaces. The fluorescent dust had a low density ($\sim$1.5 g cm^{-3}) and could mobilise into the air from the floor even after small amounts of disturbance. This is considered to be closely analogous to micro-scale particulates found in some nuclear facilities [34], although the density of nuclear particulates would be expectantly higher but with comparable electrostatic properties.

The very small amounts of leg and chassis contamination observed on the robots was determined to contribute very little to the total overall area of contamination for each platform and, hence, could be ignored for the purposes of radiation modelling. Contamination was primarily confined to traction surfaces.

From table 2, the overall contaminated surface area of the hexapod robot is considerably lower in comparison to the wheeled and tracked rovers. The difference in the total contaminated surface area between the hexapod and the other robots could be even higher if we consider that the gait mode used for the hexapod was a single leg mode where one leg is advancing at a time. Though this mode is considered safer for hexapod robots as it maintains the maximum number of legs in contact with the ground at any one time, it will also represent the gait mode with the worst contamination pick-up performance. Additionally, a relatively high speed of motion was used for the hexapod manoeuvres, thus creating a larger disturbance of the contaminated floor area. It would be possible to further reduce the contamination pick-up by adopting a slow, three-legged gait mode while covering twice the distance per complete movement cycle.

Whilst the total amount of contamination accumulated by a robot during a deployment is the primary consideration, the ease with which a robot can be decontaminated post-mission and later returned to service, is also of significant importance. The mobility design of the robots tested in this work was very different and, therefore, cleaning methods needed to be adapted for each system. For the wheeled and tracked systems, whilst smooth metal surfaces were easy to clean, any contamination in the tyre and track treads was difficult to completely remove. For real-world nuclear facilities this might mean that the robots would only be deployed once before being consigned as secondary nuclear waste objects. For the hexapod robot, replacement of the rubber ferrules on the legs enabled rapid and almost total removal of the contamination. Residual contamination on leg surfaces could be cleaned with relative ease, though some isolated particulates infiltrated and contaminated the inner parts of the hexapod's open-frame leg design. Clean-up of these surfaces would require parts of the robot to be disassembled which is highly impractical and time-consuming. It is recommended that such contamination could be mitigated by covering the hexapod with a protective sacrificial suit, which could be removed and disposed of after each deployment. Such a sustainable approach is not achievable with the other two types of robots but would represent a significant operational cost reduction if the system was reused over multiple facility deployments.

One significant advantage of the wheeled and tracked robots is that their resting positions do not change between being switched on or off. This means that scheduled or accidental robot power shutdowns will not lead to further contamination of the robot from the ground. This is not the case for the hexapod robot which is programmed to rest on the 'belly' face of the platform when power is switched off. Power shutdowns on the hexapod could be caused after a servo failure if the robot carries significant load or is operating within a deployment environment for a long period. To avoid excessive underside contamination during a power shutdown event four 30 mm long, 6 mm diameter poles were fitted to the underside of the robot to act as resting points. In this way, if the robot was mounted with a pan-tilt scanned on its top surface, it could navigate to a strategic location and the power off its leg servos for the duration of the scan without accumulating any significant contamination. These four additional points of contact are only discussed as an additional contamination safety measure and were not considered in this work. Potential addition of these points would contribute a relatively small surface area of contamination and would not affect our results significantly.

In this study the calculation of the total accumulated gamma activity for each contaminated vehicle was based on an arbitrary surface coating value of 60 kBq cm^{-2} (table 2). From table 2, it is clear that the hexapod robotic system accumulated the least radioactivity with the wheeled and tracked robot yielding comparable values. This provides a technical underpinning for the consideration that walking robots provide the optimal survey platform for radiation surveillance and mapping missions inside nuclear facilities, with quadrupeds representing an improved configuration over hexapods, and hexapods being preferable to octopods, and so on.

Using GEANT4 we were able to investigate the effects that accumulated robot radioactivity could have on a radiation detection instrument mounted on the top of each robot. The uncollimated 10 cm^3 volume CZT detector simulated in this work, represents a common type of micro gamma spectrometer used in survey applications. The modelling study clearly indicated that lower amounts of robot-accumulated radioactivity led to detector readings that would be closer to the actual radioactivity for a particular area i.e. the true radioactivity level. As the amount of contamination on the robots increased, this additional radioactivity located close to the detector added an increasing additional offset to the detector reading and, thus, a significant reduction in the accuracy of the measurements. A radiation detector mounted on a contaminated robot would provide an overestimate of the true local gamma radiation and this would need to be corrected for in post-deployment data processing. The study showed that a

way to mitigate this effect would be to raise the height of the detector, as much as practicably possible, away from the floor and away from the gamma-contaminated surfaces of the robot. This could lead to stability issues depending on the platform and the size and weight of the detector being used. Further simulation work could be performed by including other metallic components in each robot platform such as metallic casings, sensors, cameras, etc as they will scatter high energy gammas and produce secondary photons which may also affect the detector measurements. Additionally, different types of floor surfaces could be simulated in order to assess how backscatter of contamination might affect the gamma detection results in general.

The GEANT4 modelling also indicated that the footpad design of walking robots could be minimised to limit contamination pick-up, with needle-like pads representing the smallest possible ground contact area. Accordingly, either a quadruped or hexapod design would represent optimal designs, with the former offering the least ground contact and lower power consumption, but with the hexapod offering greater stability and manoeuvrability.

This study has also highlighted that robotic survey platforms can redistribute particulate contamination during a survey mission. A robot traversing a radioactively contaminated area back into a clean one will bring with it some degree of contamination. This highlights the need for adaptive path planning on the robotic system, when deployed autonomously, to attempt to avoid highly radioactive zones within the survey area to minimise through-mission contamination. These radioactive 'hot' zones would be targeted for mapping at the end of the survey once the lower activity zones had been delineated. It is also a consideration that any tethers applied to the robotic system, either for physical recovery or data transfer, would also provide a route for spreading and redistributing substantial contamination.

Future work will seek to develop and validate sacrificial skins and coverings for walking robot platforms, examining the play-off between enhanced contamination protection versus reduced system heat-loss. Much like human nuclear workers, strenuous activity inside a sealed protective suit might expectedly lead to overheating. This is a challenge that will need to be overcome if a sustainable, reusable deployment solution is to be made available to the industry.

5. Conclusions

The extent of contamination pick-up of three different robotic vehicles (wheeled rover, tracked rover and hexapod) operating within a floor-contaminated environment was investigated in this work. The differences in accumulated contamination between robots was determined using fluorescent micro-scale dust as a surrogate for real nuclear particulates. The hexapod robotic system was proven to accumulate and spread significantly less contamination than the tracked and wheeled platforms.

From the GEANT4 modelling, it was demonstrated that the differences in the accumulated contamination between platforms would equate to significant differences in the amount of radiation detected by an on-board sensor. The wheeled and tracked robots exhibited a comparable performance which could lead to significant over-estimation of the true local-area radiation intensity during a survey. By comparison, the hexapod robot exhibited significantly lower detector offset due to its propensity to accumulate very little radioactive contamination.

By taking a control measurement of detector count intensity in a 'clean' area with minimal gamma signal, and then repeating the measurement after an active deployment, the extent of robot contamination could be determined and an offset to any survey results could be applied on the assumption that contamination occurred at the start of the deployment and remained approximately constant throughout the deployment.

This study provides substantial evidence that for robotic survey applications where the ground or surrounding surfaces are contaminated with a hazardous particulate material, a walking robot will provide the best performance for minimising the amount material pick-up. Such platforms therefore present the best technical option for post-mission decontamination and reuse.

Acknowledgments

Conflict of interest

Authors have no conflict of interest relevant to this article.

ORCID iD

A Banos ⓘ https://orcid.org/0000-0001-8688-2865

References

[1] Kas K A and Johnson G K 2020 Using unmanned aerial vehicles and robotics in hazardous locations safely *Process Saf. Prog.* **39** e12066
[2] Miura H, Watanabe A, Okugawa M, Miura T and Koganeya T 2020 Plant inspection by using a ground vehicle and an aerial robot: lessons learned from plant disaster prevention challenge in World Robot Summit 2018 *Adv. Robot.* **34** 104–18
[3] Andersson K G, Fogh C, Byrne M, Roed J, Goddard A and Hotchkiss S 2002 Radiation dose implications of airborne contaminant deposition to humans *Health Phys.* **82** 226–32
[4] Pavlovsky R, Haefner A, Joshi T, Negut V, McManus K, Suzuki E, Barnowski R and Vetter K 2018 3-D radiation mapping in real-time with the localization and mapping platform LAMP from unmanned aerial systems and man-portable configurations (arXiv:1901.05038)
[5] Tsitsimpelis I, Taylor C J, Lennox B and Joyce M J 2019 A review of ground-based robotic systems for the characterization of nuclear environments *Prog. Nucl. Energy* **111** 109–24
[6] Kawatsuma S, Fukushima M and Okada T 2012 Emergency response by robots to Fukushima-Daiichi accident: summary and lessons learned *Ind. Robot Int. J.* **39** 428–435 5
[7] Ohno K, Kawatsuma S, Okada T, Takeuchi E, Higashi K and Tadokoro S 2011 Robotic control vehicle for measuring radiation in Fukushima Daiichi Nuclear Power Plant *2011 IEEE Int. Symp. on Safety, Security, and Rescue Robotics* (IEEE) pp 38–43
[8] Nagatani K, Kiribayashi S, Okada Y, Otake K, Yoshida K, Tadokoro S, Nishimura T, Yoshida T, Koyanagi E and Fukushima M 2013 Emergency response to the nuclear accident at the Fukushima Daiichi Nuclear Power Plants using mobile rescue robots *J. Field Robot.* **30** 44–63
[9] Yoshida T, Nagatani K, Tadokoro S, Nishimura T and Koyanagi E 2014 Improvements to the rescue robot quince toward future indoor surveillance missions in the Fukushima Daiichi nuclear power plant *Field and Service Robotics* (Berlin: Springer) pp 19–32
[10] Sugisaka M 2011 Working robots for nuclear power plant disasters *5th IEEE Int. Conf. on Digital Ecosystems and Technologies (IEEE DEST 2011)* (IEEE) pp 358–61

[11] Osterhout M M 2012 *Decontamination and Decommissioning of Nuclear Facilities* (Berlin/Heidelberg, Germany: Springer Science and Business Media)

[12] Nikolic J, Burri M, Rehder J, Leutenegger S, Huerzeler C and Siegwart R 2013 A UAV system for inspection of industrial facilities *2013 IEEE Aerospace Conf.* (IEEE) pp 1–8

[13] Martin P G, Moore J, Fardoulis J S, Payton O D and Scott T B 2016 Radiological assessment on interest areas on the sellafield nuclear site via unmanned aerial vehicle *Remote Sens.* **8** 913

[14] Jordan S, Moore J, Hovet S, Box J, Perry J, Kirsche K, Lewis D and Tse Z T H 2018 State-of-the-art technologies for UAV inspections *IET Radar Sonar Navig.* **12** 151–64

[15] Connor D, Martin P and Scott T 2016 Airborne radiation mapping: overview and application of current and future aerial systems *Int. J. Remote Sens.* **37** 5953–87

[16] Bird B, Griffiths A, Martin H, Codres E, Jones J, Stancu A, Lennox B, Watson S and Poteau X 2018 A robot to monitor nuclear facilities: using autonomous radiation-monitoring assistance to reduce risk and cost *IEEE Robot. Autom. Mag.* **26** 35–43

[17] Cabrol N, Chong-Diaz G, Stoker C, Gulick V, Landheim R, Lee P, Roush T, Zent A, Lameli C H and Iglesia A J 2001 Nomad rover field experiment, Atacama Desert, Chile: 1. Science results overview *J. Geophys. Res.: Planets* **106** 7785–806

[18] Anderson R B 2015 Development of mobile platform for inventory and inspection applications in nuclear environments

[19] Oliveira A D, Silva G, da Silva A R G and Lins R G 2018 Proposal of an autonomous system for inspection of structures *WIEFP2018—4th Workshop on Innovative Engineering for Fluid Power* (*28–30 November*) (Sao Paulo, Brazil: Linköping University Electronic Press) pp 1–4

[20] Shukla A and Karki H 2016 Application of robotics in offshore oil and gas industry—a review part II *Rob. Auton. Syst.* **75** 508–24

[21] Shukla A and Karki H 2016 Application of robotics in onshore oil and gas industry—a review part I *Rob. Auton. Syst.* **75** 490–507

[22] Nayak A and Pradhan S 2014 Design of a new in-pipe inspection robot *Procedia Eng.* **97** 2081–91

[23] Guimaraes M and Lindberg J 2014 Remote controlled vehicle for inspection of vertical concrete structures *Proc. 2014 3rd Int. Conf. on Applied Robotics for the Power Industry* (IEEE) pp 1–6

[24] La Rosa G, Messina M, Muscato G and Sinatra R 2002 A low-cost lightweight climbing robot for the inspection of vertical surfaces *Mechatronics* **12** 71–96

[25] Voyles R, Abbaraju P, Choset H and Ansari A 2017 Novel Serpentine robot combinations for inspection in hard-to-reach areas of damaged or decommissioned structures-17335 *Proc., Waste Management Conf. (WM2017)*

[26] Meyer H G, Klimeck D, Paskarbeit J, Rückert U, Egelhaaf M, Porrmann M and Schneider A 2020 Resource-efficient bio-inspired visual processing on the hexapod walking robot HECTOR *PLoS One* **15** e0230620

[27] Dupeyroux J, Serres J R and Viollet S 2019 AntBot: a six-legged walking robot able to home like desert ants in outdoor environments *Sci. Robot.* **4** 8 27

[28] Kell Ideas Limited, Leo Rover 2019 (available at: www.leorover.tech)

[29] Iagnemma K and Dubowsky S 2004 Traction control of wheeled robotic vehicles in rough terrain with application to planetary rovers *Int. J. Robot. Res.* **23** 1029–40

[30] Nexus Automation Limited (available at: https://nexus18.en.ecput.com)

[31] Trossen Robotics PhantomX AX Metal Hexapod Mark III Kit Chicago, IL (available at: www.trossenrobotics.com/phantomx-ax-hexapod.aspx)

[32] P.P.C. Supplies Rodent control/rodent tracking—fluorescent rodent tracking dust (available at: www.pestfix.co.uk/fluorescent-rodent-tracking-dust.asp)

[33] Zarifi M, Guatelli S, Qi Y, Bolst D, Prokopovich D and Rosenfeld A 2019 Characterization of prompt gamma rays for *in-vivo* range verification in hadron therapy: a Geant4 simulation study *J. Phys. Conf. Ser.* **1154** 012030

[34] Jones W 2019 Atomic Weapons Establishment (AWE), Personal communication